State Feedback Control Solutions for a Mechatronics System with Variable Moment of Inertia

Alexandra-Iulia Szedlak-Stinean[1], Radu-Emil Precup[1], Stefan Preitl[1], Emil M. Petriu[2]
and Claudia-Adina Bojan-Dragos[1]

[1]*Department of Automation and Applied Informatics, Politehnica University of Timisoara,*
Bd. V. Parvan 2, 300223, Timisoara, Romania
[2]*School of Electrical Engineering and Computer Science, University of Ottawa,*
800 King Edward, K1N 6N5, Ottawa, ON, Canada

Abstract: This paper presents details regarding the design of two state feedback control (SFC) solutions for the position control of a mechatronics application represented by the Model 220 Industrial Plant Emulator. Since SFC is not effective in terms of zero steady-state control error, the SFC structure of both solutions is inserted in a control loop that contains a PID controller with or without low-pass filter. This leads to the two SFC solutions proposed in this paper and dedicated to mechatronics applications with variable moment of inertia. The PID controllers are tuned by the Modulus Optimum method to ensure high control system performance expressed as increased phase margins and improved tracking performance. The performance of the proposed SFC solutions is illustrated by case studies that deal with experimentally identified parameters in two situations, rigid body dynamics and flexible drive dynamics. Simulation and experimental results obtained for the three significant values of the moment of inertia of the load disk are given.

1 INTRODUCTION

Mechatronics systems are successfully used in many industrial and non-industrial applications because of their initial simple and robust structure. The design steps of control structures for mechatronics applications are (Isermann, 2005; Bishop, 2007): 1. accept a simplified system representation, 2. set the control system performance, 3. design the measurement instrumentation including state estimation. 4. generate dynamic behaviours in special situations, 5. develop convenient control algorithms, and 6. perform the fault diagnosis.

The mechatronics application considered in this paper is the Model 220 Industrial Plant Emulator (M220IPE) laboratory equipment, which is a complex and nonlinear device that illustrates and models industrial processes with variable inertia (ECP, 2010; Stinean et al., 2013a, 2013b). The main advantages of M220IPE are the possibility to adjust the dynamic parameters and the ability to introduce and remove non-ideal proprieties in a controlled manner. M220IPE is also advantageous from the experimental testing point of view: it does not allow

a continuous variation (during operation) of the moment of inertia, which in turn determines the validation at important operating points, and a reduced flexibility to modifications of the control algorithms.

Some well acknowledged control solutions for M22OIPE will be briefly analyzed as follows. The disturbances are estimated in (Gao et al., 2001) using an extended state observer and compensated at each sampling period. Three state observer design techniques including high-gain observers, sliding mode observers and extended state observers are discussed in (Wang and Gao, 2003). The design of a static anti-windup compensator is suggested in (Takamatsu et al., 2010) on the basis of the circle criterion that leads to numerically solved linear matrix inequalities. A data-driven design method of a PID controller and a robust feedback control designed for mechanisms with backlash are given in (Saeki and Kishil, 2011). Fuzzy and neuro-fuzzy control solutions are investigated in (Stinean et al., 2013a, 2013b, 2015).

This paper gives details on the design and implementation of two state feedback control (SFC)

solutions for M220IPE. These solutions include a PID controller with a low-pass filter in case of rigid body dynamics and a PID without filter in case of flexible drive dynamics.

This paper offers four new contributions: 1. the mathematical modelling of the servo system M220IPE and the interpretation of these models as benchmark type mathematical models (MMs), 2. the design of two SFC solutions, 3. the experimental and simulated validation of the SFC structures with PID controllers in nine case studies dedicated to the position control of M220IPE with rigid body dynamics and three case studies with flexible drive dynamics, and 4. the comparative analysis of all control structures.

This paper is structured as follows: an overview on the numerical values of the system parameters is given in the next section. The MMs in case of rigid body dynamics and flexible drive dynamics are also defined. The design and implementation of the SFC solutions are discussed in Section 3. The simulation and experimental results are presented in Section 4. A comparison of the control systems performance is included. The conclusions are offered in Section 5.

2 MODEL 220 INDUSTRIAL PLANT EMULATOR

2.1 Numerical Values of System Parameters

Since the laboratory setup built around M220IPE can only provide discontinuous changes of the moment of inertia, three case studies described briefly in (Stinean et al., 2015) have been implemented, tested by simulation and experiments and analyzed. The proposed control solutions will be designed for three significant values of the moment of inertia of the load disk, J_{load}: the initial value $J_{load,init}=0.0065kgm^2$ (without weights on the load disk), the average value $J_{load,avg}=0.01474kgm^2$ (four brass weights of 0.2 kg each), and the maximum value $J_{load,max}=0.0271kgm^2$ (four brass weights of 0.5 kg each). Based on past experience (Stinean et al., 2013a, 2013b, 2015) nine combinations between process parameters and controller parameters are possible. The following notations were used to analyze and develop the proposed control solutions:

$$J_{drive} = J_{d\_drive} + J_{w\_drive}, J_{load} = J_{d\_load}$$
$$+ J_{w\_load}, J_p = J_{p\_drive} + J_{p\_load} + J_{p\_backlash},$$
$$gr = 6n_{pd}/n_{pl}, gr' = n_{pd}/12,$$
(1)

where: J_{drive} – the inertia of the drive disk, J_{d_drive} – the inertia of the bare drive disk, drive motor, encoder, drive disk/motor belt and pulleys, J_{w_drive} – the inertia associated with the brass weights at the drive disk, J_{load} – the inertia of the load disk, J_{d_load} – the inertia of the bare load disk, disturbance motor, encoder, load disk/motor belt and pulleys, J_{w_load} – the inertia associated with the brass weights at the load disk, J_p – the pulley inertia, J_{p_drive}, J_{p_load} – the inertia associated with the pulleys in the masses assembly, $J_{p\_backlash}$ – the inertia of the backlash mechanism, gr – the drive train gear ratio, gr' – the partial gear ratio between the idler pulley assembly and the drive disk, n_{pd} – the number of teeth on bottom pulley, n_{pl} – the number of teeth on top pulley, c_1, c_2 – the drive and load friction (modelled as viscous), c_{12} – the coupled friction, and k – the rotary (torsional) spring constant. The parameters of the servo system M220IPE used in the SFC design are (ECP, 2010; Stinean et al., 2013a)

$$J_{d\_drive} = 0.00040 \text{kgm}^2, J_{d\_load} = 0.0065 \text{kgm}^2,$$
$$J_{p\_backlash} = 0.000031 \text{kgm}^2,$$
$$J_{w\_drive} = 0.0021 \text{kgm}^2 \ (4 \cdot 0.2 \text{ kg at } r_{wd} = 0.05 \text{ m}),$$
$$J_{w\_drive} = 0.00561 \text{kgm}^2 \ (4 \cdot 0.5 \text{ kg at } r_{wd} = 0.05 \text{ m}),$$
$$J_{w\_load} = 0.00824 \text{kgm}^2 \ (4 \cdot 0.2 \text{ kg at } r_{wl} = 0.1 \text{ m}),$$
$$J_{w\_load} = 0.0206 \text{kgm}^2 \ (4 \cdot 0.5 \text{ kg at } r_{wl} = 0.1 \text{ m}),$$
$$J_{p\_drive} = J_{p\_load} = 0.000008 \text{kgm}^2 \ (n_{pd} = n_{pl} = 24),$$
$$J_{p\_drive} = J_{p\_load} = 0.000039 \text{kgm}^2 \ (n_{pd} = n_{pl} = 36),$$
$$c_1 = 0.004 \text{ Nm/rad/s}, c_2 = 0.05 \text{ Nm/rad/s},$$
$$c_{12} = 0.017 \text{ Nm/rad/s}, k = 8.45 \text{ Nm/rad}.$$
(2)

2.2 Mathematical Models of M220IPE

This sub-section presents the dynamic equations used in the process MM in two situations, rigid body dynamics and flexible drive dynamics.

2.2.1 Rigid Body Dynamics

The MM of M220IPE with rigid body dynamics (ECP, 2010; Stinean et al., 2013a) is obtained from the balance equation in matrix form

$$\mathbf{J}\ddot{\boldsymbol{\theta}} + \mathbf{c}\dot{\boldsymbol{\theta}} = \mathbf{T}, \ \boldsymbol{\theta} = \begin{bmatrix} \theta_1 \\ \theta_2 \end{bmatrix}, \ \mathbf{J} = \begin{bmatrix} J_{drive}^* & 0 \\ 0 & J_{load}^* \end{bmatrix},$$
$$\mathbf{c} = \begin{bmatrix} c_{drive}^* & 0 \\ 0 & c_{load}^* \end{bmatrix}, \ \mathbf{T} = \begin{bmatrix} T_D \\ gr\,T_D \end{bmatrix}.$$
(3)

with $\theta_1 = gr\theta_2$ or $\theta_1 = gr'\theta_p$, where: θ_1 – the drive disk position, θ_2 – the load disk position, θ_p – the idler

pulleys position, J_{drive}^* – the total inertia reflected to the drive disk, J_{load}^* – the total inertia reflected to the load disk, c_{drive}^*, c_{load}^* – the total reflected friction constants, and T_D – drive torque, and the expressions of the parameters in (3)

$$
\begin{aligned}
J_{drive}^* &= J_{drive} + J_p(gr')^{-2} + J_{load}(gr)^{-2}, \\
J_{load}^* &= J_{drive}gr^2 + J_p(gr/gr')^2 + J_{load}, \\
c_{drive}^* &= c_1 + c_2(gr)^{-2}, c_{load}^* = c_1 gr^2 + c_2.
\end{aligned} \tag{4}
$$

The state-space MM of M220IPE with rigid body dynamics with θ_1 as the process output is

$$
\begin{cases} \dot{\mathbf{x}} = \mathbf{A}\,\mathbf{x} + \mathbf{B}\,\mathbf{T} \\ y = \mathbf{C}\,\mathbf{x} \end{cases}, \quad \mathbf{x} = \begin{bmatrix} \theta_1 \\ \dot{\theta}_1 \end{bmatrix}, \tag{5}
$$

with the matrix expressions

$$
\mathbf{A} = \begin{bmatrix} 0 & 1 \\ 0 & -c_{drive}^*/J_{drive}^* \end{bmatrix}, \mathbf{B} = \begin{bmatrix} 0 \\ 1/J_{drive}^* \end{bmatrix}, \mathbf{C} = [1\ 0]. \tag{6}
$$

Applying the Laplace transform to (3) and accepting zero initial conditions, the process transfer function (t.f.) is

$$
\theta_1(s)/T_D(s) = (1/J_{drive}^*)/[s(s + c_{drive}^*/J_{drive}^*)]. \tag{7}
$$

2.2.2 Flexible Drive Dynamics

The balance equation in matrix form enables the derivation of the MM of M220IPE with flexible drive dynamics (ECP, 2010; Zheng et al., 2012):

$$
\mathbf{J}\,\ddot{\boldsymbol{\theta}} + \mathbf{c}\,\dot{\boldsymbol{\theta}} + \mathbf{K}\boldsymbol{\theta} = \mathbf{T}, \ \boldsymbol{\theta} = \begin{bmatrix} \theta_1 \\ \theta_2 \end{bmatrix}, \ \mathbf{J} = \begin{bmatrix} J_{drive}^* & 0 \\ 0 & J_{load} \end{bmatrix},
$$

$$
\mathbf{c} = \begin{bmatrix} c_1 + c_{12}gr^{-2} & -c_{12}gr^{-1} \\ -c_{12}gr^{-1} & c_2 + c_{12} \end{bmatrix}, \ \mathbf{T} = \begin{bmatrix} T_D \\ 0 \end{bmatrix}, \tag{8}
$$

$$
\mathbf{K} = k\begin{bmatrix} gr^{-2} & -gr^{-1} \\ -gr^{-1} & 1 \end{bmatrix}.
$$

Considering θ_1 as the process output, the state-space MM of M220IPE with flexible drive dynamics is given in (5), with the matrices

$$
\mathbf{x} = [\theta_1\ \dot{\theta}_1\ \theta_2\ \dot{\theta}_2]^T, \ \mathbf{A} = [a_{ij}]_{i,j=1\dots4},
$$
$$
\mathbf{B} = [b_{i1}]_{i=1\dots4}, \ \mathbf{C} = [1\ 0\ 0\ 0], \tag{9}
$$

with the matrix elements

$$
\begin{aligned}
& a_{11} = 0, a_{12} = 1, a_{13} = 0, a_{14} = 0, \\
& a_{21} = -kgr^{-2}/J_{drive}^*, a_{22} = -(c_1 + c_{12}gr^{-2})/J_{drive}^*, \\
& a_{23} = kgr^{-1}/J_{drive}^*, a_{24} = c_{12}gr^{-1}/J_{drive}^*, a_{31} = 0, \\
& a_{32} = 0, a_{33} = 0, a_{34} = 1, a_{41} = kgr^{-1}/J_{load}, \\
& a_{42} = c_{12}gr^{-1}/J_{load}, a_{43} = -k/J_{load}, a_{44} = -(c_2 \\
& + c_{12})/J_{load}, b_{11} = 0, b_{21} = 1/J_{drive}^*, b_{31} = 0, b_{41} = 0.
\end{aligned} \tag{10}
$$

Applying the Laplace transform to (8) and accepting zero initial conditions, the process t.f. is

$$
\begin{aligned}
& \theta_1(s)/T_D(s) = [J_{load}s^2 + (c_2 + c_{12})s + k]/D(s), \\
& D(s) = n_4 s^4 + n_3 s^3 + n_2 s^2 + n_1 s + n_0, \\
& n_4 = J_{drive}^* J_{load}, \ n_3 = J_{drive}^*(c_2 + c_{12}) + J_{load}[c_1 \\
& + c_{12}/(gr^2)], \ n_2 = J_{drive}^* k + J_{load}k/(gr^2) + c_1 c_2 \\
& + c_1 c_{12} + c_{12}c_2/(gr^2), \ n_1 = c_1 k + c_2 k/(gr^2), \\
& n_0 = 0.
\end{aligned} \tag{11}
$$

The t.f.s given in (7) and (11) and the matrix coefficients for three significant values of the moment of inertia of the load disk are given in Tables 1 and 2.

3 STATE FEEDBACK CONTROL SOLUTIONS

3.1 Classical SFC Solutions

The SFC structure is illustrated as the internal control loop in Figure 1. It is next extended and included in a control loop with a PID controller in order to ensure a zero steady-state control error as discussed in sub-section 3.2. The state feedback gain matrix $\mathbf{k_c^T}$ in both situations is of proportional type.

The state feedback controller includes an additional amplifier with the gain set to $k_{AS}=1$. Figure 1 leads to

$$
e_x = w_x - y_x, u = k_{AS}e_x. \tag{12}
$$

The pole placement method is applied to compute $\mathbf{k_c^T}$ using three sets of poles imposed, each for the three significant values of the moment of inertia of the load disk, i.e., $J_{load,init}$, $J_{load,avg}$, $J_{load,max}$. The notation $y_x = \mathbf{k_c^T x}$ is used in Figure 1. This leads to the state-space MM of the SFC structure

$$
\begin{cases} \dot{\mathbf{x}} = \mathbf{A_x}\,\mathbf{x} + \mathbf{B}\,k_{AS}w_x \\ y = \mathbf{C}\,\mathbf{x} \end{cases}, \ \mathbf{A_x} = \mathbf{A} - \mathbf{B}\,\mathbf{k_c^T}k_{AS}, \tag{13}
$$

where $\mathbf{A_x}$ is the matrix of the inner SFC loop. The state feedback gain matrix of M220IPE with rigid body dynamics is according to Table 3, columns 4 and 5 and the state feedback gain matrix of M220IPE with flexible drive dynamics is according to Table 3, columns 10, 11, 12 and 13. The closed-loop system poles (i.e., the inner SFC loop) are given Table 3, columns 2 and 3 for rigid body dynamics and in columns 6, 7, 8 and 9 for flexible drive dynamics. The t.f. of the inner SFC loop is

$$H_{SFC}(s) = \mathbf{C}(s\mathbf{I} - \mathbf{A}_x)^{-1}\mathbf{B}$$

$$= \begin{cases} \dfrac{k_{SFC}}{(1+T_1 s)(1+T_2 s)} \quad or \\ \dfrac{k_{SFC}(1+2\zeta_b T_b s + T_b^2 s^2)}{(1+T_1 s)(1+T_2 s)(1+T_3 s)(1+T_4 s)}, \end{cases} \quad (14)$$

where $\mathbf{I}$ is the second-order (or fourth-order) identity matrix, k_{SFC} is the inner SFC loop gain, T_1 (or T_1, T_2) is (are) the large time constant, and T_2 (or T_3, T_4) is (are) the small time constant (s).

3.2 Design and Implementation of PID Controllers

The first SFC solution uses a PID controller with a low-pass filter with the generic t.f. and parameters

$$H_c(s) = (k_c / s)(1 + sT_{c1})(1 + sT_{c2})$$
$$/(1 + sT_f), k_c = 1/(2k_{SFC}T_2), \quad (15)$$
$$T_{c1} = T_1, T_{c2} = T_2, T_f = 0.9T_{c2},$$

where k_c is the controller gain, T_{c1} and T_{c2} are the controller time constants, and T_f is the filter time constant. The control algorithm is designed and tuned in terms of Kessler's Modulus Optimum method (MO-m) referred in (Åström and Hägglund, 1995).

Using the backwards difference method, the continuous-time PID controller with the continuous-time t.f. $H_c(s)$ is discretized resulting in the discrete-time t.f. $H_c(z^{-1})$

$$H_c(z^{-1}) = \frac{q_0 + q_1 z^{-1} + q_2 z^{-2}}{p_0 + p_1 z^{-1} + p_2 z^{-2}},$$
$$q_0 = k_c(T_{c1} + T_s)(T_{c2} + T_s), q_2 = k_c T_{c1} T_{c2}, \quad (16)$$
$$q_1 = -k_c[T_{c1}(T_{c2} + T_s) + T_{c2}(T_{c1} + T_s)],$$
$$p_0 = T_f + T_s, p_1 = -(2T_f + T_s), p_2 = T_f,$$

where $T_s = 0.004$s is the sampling period. The numerical values related to SFC structure and the PID controllers for three significant operating points are given in Table 4.

Table 1: State-space MM matrices and transfer functions expressions of M220IPE with rigid body dynamics.

Moment of inertia	Matrices $\mathbf{A}$, $\mathbf{B}$ and $\mathbf{C}$	Process transfer function $\theta_1(s)/T_D(s)$
$J_{load,init}$	$\mathbf{A} = \begin{bmatrix} 0 & 1 \\ 0 & -8.63 \end{bmatrix}, \mathbf{B} = \begin{bmatrix} 0 \\ 7036 \end{bmatrix}, \mathbf{C} = \begin{bmatrix} 1 & 0 \end{bmatrix}$	$\dfrac{7036}{s(s+8.63)}$
$J_{load,avg}$	$\mathbf{A} = \begin{bmatrix} 0 & 1 \\ 0 & -5.35 \end{bmatrix}, \mathbf{B} = \begin{bmatrix} 0 \\ 4362 \end{bmatrix}, \mathbf{C} = \begin{bmatrix} 1 & 0 \end{bmatrix}$	$\dfrac{4362}{s(s+5.35)}$
$J_{load,max}$	$\mathbf{A} = \begin{bmatrix} 0 & 1 \\ 0 & -3.37 \end{bmatrix}, \mathbf{B} = \begin{bmatrix} 0 \\ 2741 \end{bmatrix}, \mathbf{C} = \begin{bmatrix} 1 & 0 \end{bmatrix}$	$\dfrac{2741}{s(s+3.37)}$

Table 2: State-space MM matrices and transfer functions expressions for M220IPE with flexible drive dynamics.

Moment of inertia	Matrices $\mathbf{A}$, $\mathbf{B}$ and $\mathbf{C}$	Process transfer function $\theta_1(s)/T_D(s)$
$J_{load,init}$	$\mathbf{A} = \begin{bmatrix} 0 & 1 & 0 & 0 \\ -1259 & -12.068 & 5036 & 10.13 \\ 0 & 0 & 0 & 1 \\ 325 & 0.654 & -1300 & -10.307 \end{bmatrix}, \mathbf{B} = \begin{bmatrix} 0 \\ 13850 \\ 0 \\ 0 \end{bmatrix}, \mathbf{C} = \begin{bmatrix} 1 & 0 & 0 & 0 \end{bmatrix}$	$\dfrac{13850(s^2 + 10.307s + 1300)}{s(s^3 + 22.37s^2 + 2677.2s + 22078)}$
$J_{load,avg}$	$\mathbf{A} = \begin{bmatrix} 0 & 1 & 0 & 0 \\ -1259 & -12.068 & 5036 & 10.13 \\ 0 & 0 & 0 & 1 \\ 145 & 0.3 & -579 & -4.59 \end{bmatrix}, \mathbf{B} = \begin{bmatrix} 0 \\ 13850 \\ 0 \\ 0 \end{bmatrix}, \mathbf{C} = \begin{bmatrix} 1 & 0 & 0 & 0 \end{bmatrix}$	$\dfrac{13850(s^2 + 4.59s + 579)}{s(s^3 + 16.65s^2 + 1893.7s + 9827.4)}$
$J_{load,max}$	$\mathbf{A} = \begin{bmatrix} 0 & 1 & 0 & 0 \\ -1259 & -12.068 & 5036 & 10.13 \\ 0 & 0 & 0 & 1 \\ 77.9 & 0.157 & -312 & -2.47 \end{bmatrix}, \mathbf{B} = \begin{bmatrix} 0 \\ 13850 \\ 0 \\ 0 \end{bmatrix}, \mathbf{C} = \begin{bmatrix} 1 & 0 & 0 & 0 \end{bmatrix}$	$\dfrac{13850(s^2 + 2.47s + 312)}{s(s^3 + 14.53s^2 + 1599.4s + 5290.4)}$
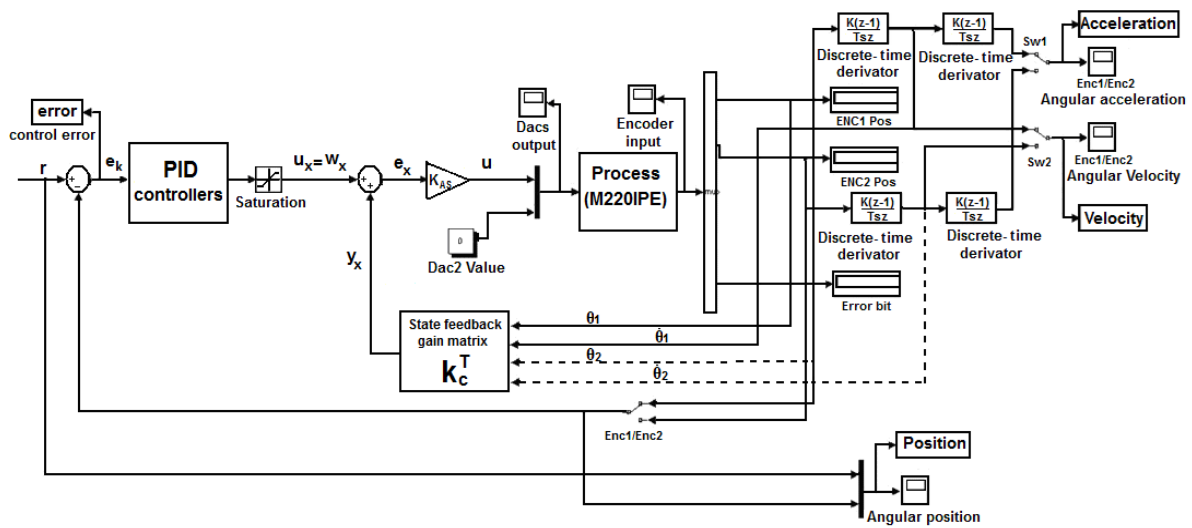
Figure 1: Control structure of M220IPE with rigid body dynamics and flexible drive dynamics.

Table 3: Selected poles and state feedback gain matrix numerical values.

Moment of inertia	Rigid body dynamics				Flexible drive dynamics							
	Selected poles		State feedback gain matrix		Selected poles				State feedback gain matrix			
1	2	3	4	5	6	7	8	9	10	11	12	13
	p_1^*	p_2^*	k_{c1}	k_{c2}	p_1^*	p_2^*	p_3^*	p_4^*	k_{c1}	k_{c2}	k_{c3}	k_{c4}
$J_{load,init}$	-20	-11	0.0313	0.0032	-20	-11	-105	-110	0.9735	0.0161	-3.3304	-0.0036
$J_{load,avg}$	-20	-7	0.0321	0.0050	-20	-7	-50	-55	0.2385	0.0083	-0.7600	0.0002
$J_{load,max}$	-20	-5	0.0365	0.0079	-20	-5	-30	-35	0.0712	0.0054	-0.1873	0.0018

Table 4: SFC structure t.f.s and numerical values of PID controllers' parameters for rigid body dynamics.

Moment of inertia	SFC structure t.f. $H_{SFC}(s)$	Parameters of PID controllers					
		q_0	q_1	q_2	p_0	p_1	p_2
$J_{load,init}$	$\dfrac{31.9818}{(1+0.0909s)(1+0.05s)}$	0.0016	-0.0030	0.0014	0.0490	-0.0940	0.0450
$J_{load,avg}$	$\dfrac{31.1571}{(1+0.1429s)(1+0.05s)}$	0.0025	-0.0048	0.0023	0.0490	-0.0940	0.0450
$J_{load,max}$	$\dfrac{27.41}{(1+0.2s)(1+0.05s)}$	0.0040	-0.0077	0.0036	0.0490	-0.0940	0.0450

Since the M220IPE with flexible drive dynamics is a fourth-order system, the second SFC solution uses a PID controller to compensate two large time constants. The generic continuous-time t.f. of the PID controller is given in (15). The requirement to ensure zero steady-state control error is fulfilled by the I component of the PID controller. The MO-m is also applied to tune the three PID controllers with fixed parameter values. Setting the value of the sampling period to T_s=0.004s, the continuous-time PID controller is discretized using the backwards difference method and the discrete-time parameters

q_0, q_1 and q_2 are according to relation (16), the only differences are in p_0 and p_1 (p_0=T_s and p_1=$-T_s$) parameters. The numerical values of the parameters of the PID controllers used in simulations and experiments are presented in Table 5.

4 SIMULATION AND EXPERIMENTAL RESULTS

The two SFC solutions described in Section 3 have

Table 5: SFC structure t.f.s and numerical values of PID controllers' parameters for flexible drive dynamics.

Moment of inertia	SFC structure t.f. $H_{SFC}(s)$	Parameters of PID controllers				
		q_0	q_1	q_2	p_0	p_1
$J_{load,init}$	$\dfrac{7.0838(1+0.0079s+0.00077s^2)}{(1+0.0909s)(1+0.05s)(1+0.0095s)(1+0.0091s)}$	0.0038	-0.0072	0.0034	0.0040	-0.0040
$J_{load,avg}$	$\dfrac{20.8286(1+0.0079s+0.0017s^2)}{(1+0.1429s)(1+0.05s)(1+0.02s)(1+0.0182s)}$	0.0040	-0.0075	0.0036	0.0040	-0.0040
$J_{load,max}$	$\dfrac{41.0952(1+0.0079s+0.0032s^2)}{(1+0.2s)(1+0.05s)(1+0.0333s)(1+0.0286s)}$	0.0028	-0.0053	0.0025	0.0040	-0.0040

Table 6: Performance indices achieved by the control systems with PID controllers.

Case study 1.1			Case study 1.2			Case study 1.3		
σ_1	t_1	t_s	σ_1	t_1	t_s	σ_1	t_1	t_s
5.05%	0.2209	0.4928	18.75%	0.266	0.7717	20.625%	0.3281	0.8898
Case study 2.1			Case study 2.2			Case study 2.3		
σ_1	t_1	t_s	σ_1	t_1	t_s	σ_1	t_1	t_s
1%	0.1867	1.3021	12.5%	0.2306	0.6901	15%	0.2806	0.7202
Case study 3.1			Case study 3.2			Case study 3.3		
σ_1	t_1	t_s	σ_1	t_1	t_s	σ_1	t_1	t_s
17.1%	0.1236	1.4997	16.99%	0.1707	1.2411	13%	0.2428	0.7625
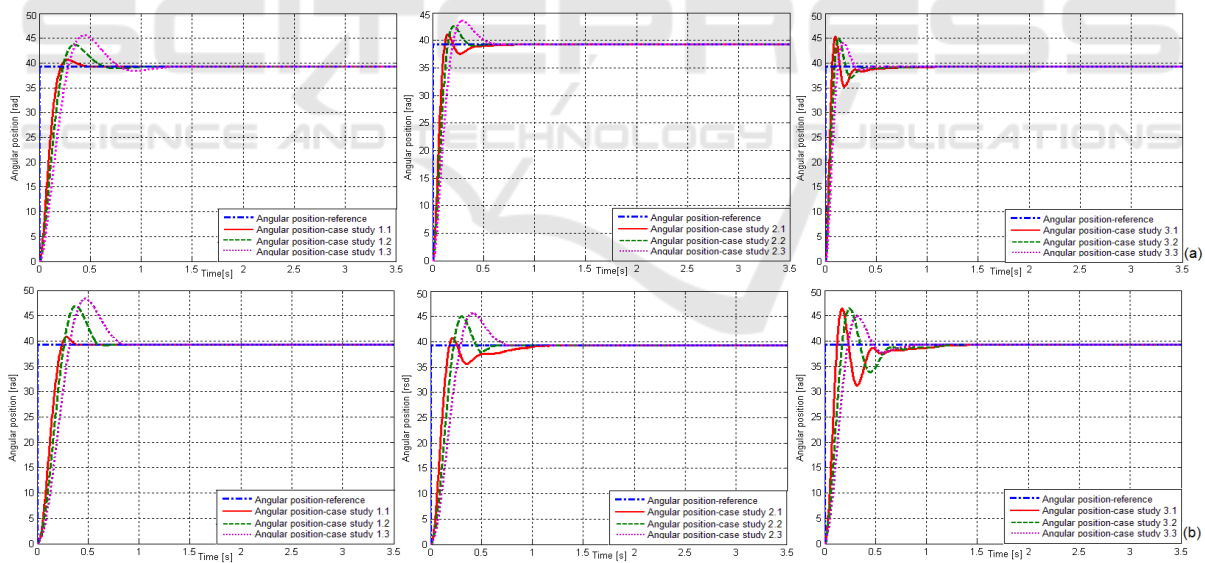
Figure 2: Simulation (a) and experimental (b) results regarding the behaviour of SFC structures with PID controllers designed for M220IPE with rigid body dynamics: case studies 1.1-1.3, 2.1-2.3 and 3.1-3.3.
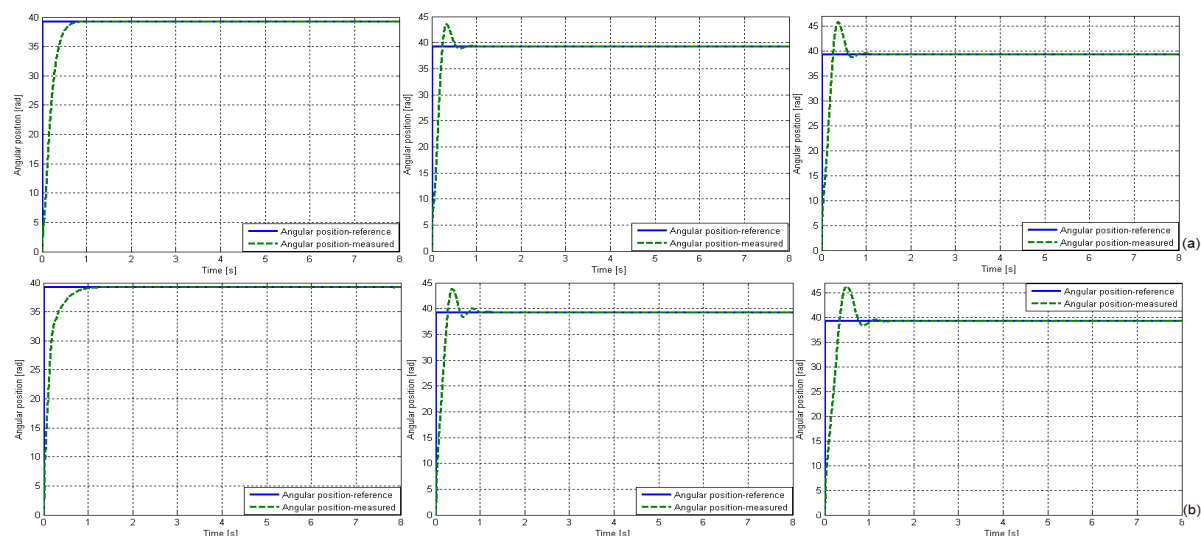
Figure 3: Simulation (q) and experimental (b) results regarding the behaviour of SFC structures with PID controllers developed for M220IPE with flexible drive dynamics: case study 1.1, 2.2 and 3.3.

been implemented and tested on M220IPE laboratory as position control systems. The results obtained on the M220IPE laboratory equipment with rigid body dynamics are presented in Figure 2. Three SFC structures – each for every moment of inertia of the load disk – have been tested on the nonlinear system and validated by simulation and real-time experiments. Analyzing the comparative results illustrated in Figure 2 and the performance synthesized in Table 6 for the experimental results, it can be concluded that the best reference tracking and control system performance has been obtained in the case studies 1.1, 2.2 and 3.3.

The three most favourable case studies were tested for M220IPE with flexible drive dynamics, and the results are presented in Figure 3. Both simulation and experimental results show similar performance indices in terms of the settling time values, the first settling time values and the overshoot values as follows: case study 1.1: $\sigma_1 \approx 0\%$, $t_1 \approx 0.934$s, $t_s \approx 1$s; case study 2.2: $\sigma_1 \approx 11.25\%$, $t_1 \approx 0.252$s, $t_s \approx 1.2308$s; case study 3.3: $\sigma_1 \approx 15.5\%$, $t_1 \approx 0.267$s, $t_s \approx 1.3916$s. The analysis of the set of results presented for the two SFC solutions points out that all tested control solutions provide relatively good reference tracking. The comparative results given in Figures 2 and 3 prove that the PID controllers contribute in average to both good dynamic performance and robustness with respect to at least one process parameter.

5 CONCLUSIONS

This paper has given design and implementation

details on two SFC solutions for a mechatronics application with rigid body dynamics and flexible drive dynamics for three significant values of the moment of inertia on the load disk. The simulation and real-time experimental results show that our SFC structures exhibit good control system performance indices that should be improved in critical applications. The main advantages of the new results given in this paper are the simplicity of the SFC structure with a reduced number of parameters and the transparency of the design approach.

Our SFC solutions can be viewed as a support for other control solutions including fuzzy, neural, sliding mode and adaptive control (Blažič et al., 2010; Precup et al., 2009, 2012; Ruano et al., 2002). The performance can be improved by inserting sensitivity, robustness objectives and constraints (Casavola et al., 2014; Gutiérrez-Carvajal et al., 2016). The pole placement method applied in this paper can be replaced by the optimal design and tuning by means of classical or modern optimization algorithms (Bandarabadi et al., 2015; Johanyák, 2015; Menchaca-Mendez and Coello Coello, 2016). This has not been investigated, but it represents a subject of future research. Future research will also be focused on applications to other illustrative nonlinear processes.

ACKNOWLEDGEMENTS

REFERENCES

Åström, K. J., Hägglund, T., 1995. *PID Controllers Theory: Design and Tuning*. Research Triangle Park, NC: Instrument Society of America.

Bandarabadi, M., Rasekhi, J., Teixeira, C. A., Netoff, T. I., Parhi, K. K., Dourado, A., 2015. Early seizure detection using neuronal potential similarity: a generalized low-complexity and robust measure. *International Journal of Neural Systems*. 25, 1-18.

Bishop, R. H., 2007. *The Mechatronics Handbook.* Boca Raton, FL: CRC Press, 2nd edition.

Blažič, S., Matko, D., Škrjanc, I., 2010. Adaptive law with a new leakage term. *IET Control Theory & Applications*. 4, 1533-1542.

Casavola, A., Garone, E., Tedesco, F., 2014. Improved feed-forward command governor strategies for constrained discrete-time linear systems. *IEEE Transactions on Automatic Control*. 59, 216-223.

ECP (2010). *Industrial Emulator/Servo Trainer Model 220 System, Testbed for Practical Control Training*. Bell Canyon, CA: Educational Control Products.

Gao, Z., Hu, S., Jiang, F., 2001. A novel motion control design approach based on active disturbance rejection. In *Proceedings of 40th IEEE Conference on Decision and Control*. Orlando, FL, USA, 5, 4877-4882.

Gutiérrez-Carvajal, R. E., de Melo, L. F., Rosário, J. M., Tenreiro Machado, J. A., 2016. Condition-based diagnosis of mechatronic systems using a fractional calculus approach. *International Journal of Systems Science*. 47, 2169-2177.

Isermann, R., 2005. *Mechatronic Systems: Fundamentals*. Berlin, Heidelberg, New York: Springer-Verlag.

Johanyák, Z. C., 2015. A simple fuzzy logic based power control for a series hybrid electric vehicle. In *Proceedings of 9th IEEE European Modelling Symposium on Mathematical Modelling and Computer Simulation*. Madrid, Spain, 207-212.

Menchaca-Mendez, A., Coello Coello, C. A., 2016. Selection mechanisms based on the maximin fitness function to solve multi-objective optimization problems. *Information Sciences*. 332, 131-152.

Precup, R.-E., Dragos, C.-A., Preitl, S., Radac, M.-B.,

Petriu, E. M., 2012. Novel tensor product models for automatic transmission system control. *IEEE Systems Journal*. 6, 488–498.

Precup, R.-E., Tomescu, M. L., Preitl, S., 2009. Fuzzy logic control system stability analysis based on Lyapunov's direct method. *International Journal of Computers, Communication & Control*. 4, 415–426.

Ruano, A. E. B., Cabrita, C., Oliveira, J. V., Kóczy, L. T., 2002. Supervised training algorithms for B-Spline neural networks and neuro-fuzzy systems. *International Journal of Systems Science*. 33, 689-711.

Saeki, M., Kishi, R., 2011. A data-driven PID control design by linear programming for stable plants. In *Proceedings of 18th IFAC World Congress*. Milano, Italy, 7420-7425.

Stinean, A.-I., Bojan-Dragos, C.-A., Precup, R.-E., Preitl, S., Petriu, E. M., 2015. Takagi-Sugeno PD+I fuzzy control of processes with variable moment of inertia. In *Proceedings of 2015 International Symposium on Innovations in Intelligent Systems and Applications*. Madrid, Spain, 1-8.

Stinean, A.-I., Preitl, S., Precup, R.-E., Dragos, C.-A., Radac, M.-B., Petriu, E. M., 2013a. Modeling and control of an electric drive system with continuously variable reference, moment of inertia and load disturbance. In *Proceedings of 9th Asian Control Conference*. Istanbul, Turkey, 1-6.

Stinean, A.-I., Preitl, S., Precup, R.-E., Dragos, C.-A., Radac, M.-B., Petriu, E. M., 2013b. Low-cost neuro-fuzzy control solution for servo systems with variable parameters. In *Proceedings of 2013 IEEE International Conference on Computational Intelligence and Virtual Environments for Measurement Systems and Applications*. Milano, Italy, 156-161.

Takamatsu, S., Wasiwitono, U., Saeki, M., Wada, N., 2010. Anti-windup compensator design considering behavior of controller state. In *Proceedings of 2010 IEEE International Conference on Control Applications*. Yokohoma, Japan, 1963-1968.

Wang, W., Gao, Z., 2003. A comparison study of advanced state observer design techniques. In *Proceedings of 2003 American Control Conference*. Denver, CO, USA, 6, 4754-4759.

Zheng, Q., Gao, L. Q., Gao, Z., 2012. On validation of extended state observer through analysis and experimentation. *Journal of Dynamic Systems, Measurement, and Control*. 134, 024505.1–024505.6.